Hindawi
Mathematical Problems in Engineering
Volume 2023, Article ID 3468295, 12 pages
https://doi.org/10.1155/2023/3468295

Research Article

Accelerating Flow of Carbon Nanotubes with Carboxymethyl Cellulose and Blood Base Materials with Comparative Thermal Features: Prabhakar Fractional Model

Ali Raza,[1] **Kamel Al-Khaled**,[2] **Taseer Muhammad**,[3] **and Sami Ullah Khan**[4]

[1]*Department of Mathematics, University of Engineering and Technology, Lahore 54890, Pakistan*
[2]*Department of Mathematics & Statistics, Jordan University of Science and Technology, P.O. Box 3030, Irbid 22110, Jordan*
[3]*Department of Mathematics, College of Sciences, King Khalid University, Abha 61413, Saudi Arabia*
[4]*Department of Mathematics, COMSATS University Islamabad, Sahiwal 57000, Pakistan*

Correspondence should be addressed to Taseer Muhammad; taseer_qau@yahoo.com

Received 23 June 2022; Revised 23 August 2022; Accepted 12 December 2022; Published 14 January 2023

Academic Editor: Albert Alexander Stonier

A fractional model is developed to investigate the thermal onset of carbon nanotubes containing single-wall carbon nanotubes (SWCNTs) and multiwall carbon nanotubes (MWCNTs). The blood and carboxymethyl cellulose (CMC) are utilized to report the characteristics of the base material. The thermal phenomenon is further supported with inclined magnetic force and mixed convection features. The vertical plate with an oscillatory nature induced the flow. After formulating the problem in view of flow assumptions, the fractional framework is carried out via the Prabhakar technique. The validation of the fractional model is ensured in view of previous studies. The comparative thermal aspect of carbon nanotubes and base materials by varying flow parameters is tested.

1. Introduction

The recent trend in thermal engineering proposes a cheaper source of energy based on the utilization of nanoparticles in the current century. The thermal mechanism of various base fluids is usually lower and less stable. The continued work in nanotechnology has experimentally proven that base materials' thermal onset can be improved when nanomaterials are immersed in a proper way. The nanoparticles are low sized metallic particles which reports exclusively enhanced thermal impact. Recent applications of nanomaterials are commonly noticed in thermal management systems, chemical processes, as a heating source in industries, solar systems, extrusion processes, etc. The work on nanofluids was initiated by Choi [1], and it is being further extended in different directions by scientists. Turkyilmazoglu [2] discussed different thermal aspects of nanofluids with the implementation of a single-phase model and tested their stability properties. Ahmad et al. [3] incorporated the insight thermal onset of micropolar nanofluid by incorporating the modified heat flux relations. Thumma et al. [4] observed the optimized contribution of nanofluid with wall-heated properties. The binary chemical flow regarding the nanofluid flow was addressed in the continuation of Abbasi et al. [5]. Rasool et al. [6] intended the nanofluid flow to be subjected to the Darcy–Forchheimer phenomenon. The isothermal conducting flow of Maxwell nanofluid with the contribution of Lorentz forces has been depicted by Rasool et al. [7]. Shafiq et al. [8] investigated the Casson fluid properties due to nanofluids with magnetic force impact. Ali et al. [9] observed the elongated surface moving flow subject to hybrid nanofluids along with the rotation phenomenon. Mahesh et al. [10] approached the non-Fourier framework for nanofluid flow in view of entropy generation applications.

In contrast to simple materials, carbon nanotubes (CNTs) report more impressive thermal impact and stable properties like electrical and thermal conductivities, density,

dimensions, and size. In fact, carbon nanotubes (CNTs) are taken as cylindrical molecules consisting of rolled-up sheets of carbon atoms with a single layer. The CNTs are classified as single-walled carbon nanotubes (SWCNT) and multi-walled carbon nanotubes (MWCNT). The diameter of SWCNT is usually less than one nm, while the diameter of (MWCNT) is approaching 100 nm. Different aspects of CNTs have been studied by researchers with diverse flow features. Reddy et al. [11] discussed the cavity flow due to the uniform distribution of CNTs along with optimized consequences. Noranuar et al. [12] evaluated the rotating orientation of CNTs with Casson fluid following the disc flow. Imtiaz et al. [13] reported the fluctuated thickness features for CNTs with bidirectional moving regime. The heating object on the enclosure with CNT distribution has been depicted in the continuation of Vishnu Ganesh et al. [14]. Shoaib et al. [15] worked out the neural computing investigation for a CNTs problem. Alzahrani and Ijaz Khan [16] focused on the coating simulation of CNTs' flow with the contribution of Wu's slip evaluation.

The fractional research provides modern tools of computations for performing the analytical and numerical simulations. The widely work in the area of fractional mathematics, different algorithms are defined by researchers. Such tools are important to define the solution to differential and integral problems. The motivations and valuable applications of such tools are associated with the computation of various problems in engineering, industrial development, thermal engineering, chemistry, physics, bioengineering, and the computational sciences. After focusing on different fractional tools, it is observed that the Caputo and Fabrizio (CF) technique is the first interesting and novel fractional definition, which has been widely used by researchers for different problems [17–19]. Atangana and Baleanu [20] provided a new type of fractional algorithm with a stronger approach. The AB tools provide a modification of the CF approach and enable simulations for nonsingular kernels [21–24]. In different fractional studies, the Prabhakar fractional approach is another analytical framework that is not focused in a comprehensive way. The distinct aspect of this fractional approach is the assessment of the odd behavior of a fluctuating person with a nonlocal kernel. Following this definition, the nonsingular and nonlocal kernel problems can be effectively treated [25–27].

The current investigation provides fractional simulations for oscillating flows of carbon nanotubes to improve the thermal properties of blood and carboxymethyl cellulose (CMC)-based fluids. The thermal classification of CNTs is observed by using single-wall carbon nanotubes (SWCNTs) and multiwall carbon nanotubes (MWCNTs). The mixed convection features are attributed to natural convection flow. The fractional computations are performed via the Prabhakar fractional model. This model provides answers to the following research questions:

(i) How carbon nanotubes (CNTs) with SWCNTs and MWCNTs are effective to enhance the thermal measurement of blood and carboxymethyl cellulose (CMC)?

(ii) Referring to blood and CMC base materials, which material reports more impressive thermal performances with the interaction of CNTs?

(iii) How a mathematical model based on the basic definition of Prabhakar fractional technique is developed?

(iv) Which nanomaterial reports a more stable thermal impact associated with the CMC-SWCNTs and CMC-MWCNTs interactions?

(v) What is the role of magnetic force and mixed convection phenomenon in enhancing the thermal transportation process.

(vi) For accelerating flow, how are slip effects important to control the flow?

2. Flow Model with Governing Equations

The thermal impact of CNTs with SWCNTs and MWCNTs is focused. The uniform suspension of SWCNTs and MWCNTs along with blood and carboxymethyl cellulose (CMC) is considered. The oscillating surface flow caused the vertically accelerating flow. The inclined direction along angle θ is considered to incorporate the magnetic force impact. The flow pattern is based on time-dependent flow. The base fluid properties are notified via viscoelastic flow model. The vertical plate oscillates with velocity $H(t)\mathrm{Cos}(\omega t)$ with uniform frequency ω. The stream temperature and concentrations are T_∞ and C_∞, respectively. The flow model using such assumptions is developed in the following set of equations:

Momentum equation:

$$\left(\frac{\partial u_{(\xi,t)}}{\partial t}-\beta_1^*\frac{\partial^3 u_{(\xi,t)}}{\partial t\partial \mathbf{y}^2}\right)=\frac{\mu_{nf}}{\rho_{nf}}\frac{\partial^2 u_{(\xi,t)}}{\partial \boldsymbol{\xi}^2}-\frac{\sigma_{nf}B_o^2}{\rho_{nf}}\sin(\theta_1)u_{(\xi,t)}+g(\beta_T)_{nf}\left(T_{(\xi,t)}-T_\infty\right)+g(\beta_c)_{nf}\left(C_{(\xi,t)}-C_\infty\right). \tag{1}$$

Thermal equation:

$$\left(\rho C_p\right)_{nf}\frac{\partial T_{(\xi,t)}}{\partial t}=-\frac{\partial q_{(\xi,t)}}{\partial \boldsymbol{\xi}}. \tag{2}$$

Fourier law of thermal flux:

$$q_{(\xi,t)}=-(k)_{nf}\frac{\partial T_{(\xi,t)}}{\partial \boldsymbol{\xi}}. \tag{3}$$

Diffusion balance equation:

$$\frac{\partial C_{(\xi,t)}}{\partial t}=-\frac{\partial J_{(\xi,t)}}{\partial \boldsymbol{\xi}}. \tag{4}$$

Fick's law:

$$J_{(\xi,t)}=-D\frac{\partial T_{(\xi,t)}}{\partial \boldsymbol{\xi}}. \tag{5}$$

The oscillating boundary constraints for slip flow are as follows:

$$\begin{aligned} u_{(\xi,0)} &= 0, \\ T_{(\xi,0)} &= T_\infty, \\ C_{(\xi,0)} &= C_\infty; \forall \xi \geq 0, \\ u_{(0,t)} - h\left.\frac{\partial u}{\partial \xi}\right|_{\xi=0} &= U_o H(t) f(t), \\ \left.\frac{\partial T}{\partial \xi}\right|_{\xi=0} &= -\frac{h}{k} T_{(0,t)}, \\ C_{(0,t)} = C_w; \quad t > 0 u_{(\xi,t)} &\longrightarrow 0,\ T_{(\xi,t)} \longrightarrow T_\infty, C_{(\xi,t)} \longrightarrow C_\infty;\ \xi \longrightarrow \infty, t > 0. \end{aligned} \tag{6}$$

The mathematical formulae for distinct flow characteristics is notified via Table 1.

Following below dimensionless variables:

$$\begin{aligned} \xi^* &= \frac{\xi \mathrm{h}}{k}, \\ u^* &= \frac{u\nu}{g(k/h)^2}, \\ t^* &= \frac{t\nu}{(k/h)^2}, \\ T^* &= \frac{T_{(\xi,t)} - T_\infty}{T_w - T_\infty}, \\ q^* &= \frac{q}{q_o}, \\ C^* &= \frac{C_{(\xi,t)} - C_\infty}{C_w - C_\infty}, \\ \mathrm{Pr} &= \frac{\mu C_p}{\kappa}, \\ Gr &= \frac{g(\upsilon\beta_T)_f (T_\infty)}{\nu^2}, \\ M &= \frac{\sigma_f \upsilon_f B_o^2}{\rho_f U_o^2}, \\ Gm &= \frac{g(\upsilon\beta_C)_f (C_\infty)}{\nu^2}, \\ \beta_1 &= \frac{\beta_1^* g}{\nu^2 \rho}\left(\frac{k}{\mathrm{h}}\right), \end{aligned} \tag{7}$$

with Prandtl number Pr, heat Grashof number Gr, mass Grashof number Gm, magnetic constant M, and viscoelastic parameter β_1. The dimensionless system in view of defined variables is as follows:

$$\begin{aligned} \frac{\partial}{\partial t}\left(u_{(\xi,t)} - \beta_1 \frac{\partial^2 u_{(\xi,t)}}{\partial \xi^2}\right) &= \frac{\partial^2 u_{(\xi,t)}}{\partial \xi^2} - M \sin(\theta_1) u_{(\xi,t)} \\ &\quad + Gr\, T_{(\xi,t)} + Gm\, C_{(\xi,t)}, \end{aligned} \tag{8}$$

$$\mathrm{Pr}\frac{\partial T_{(\xi,t)}}{\partial t} = -\frac{\partial q_{(\xi,t)}}{\partial \xi}, \tag{9}$$

$$Sc\frac{\partial C_{(\xi,t)}}{\partial t} = -\frac{\partial J_{(\xi,t)}}{\partial \xi}, \tag{10}$$

with:

$$
\begin{aligned}
u_{(\xi,0)} &= 0,\\
T_{(\xi,0)} &= 0,\\
C_{(\xi,0)} &= 0,\\
u_{(0,t)} - h\frac{\partial u}{\partial \xi}\bigg|_{\xi=0} &= H(t)f(t),\\
\frac{\partial T}{\partial \xi}\bigg|_{\xi=0} &= -\left(1 + T_{(0,t)}\right),\\
C_{(0,t)} &= 1\, u_{(\xi,t)} \longrightarrow 0, T_{(\xi,t)} \longrightarrow 0, C_{(\xi,t)} \longrightarrow 0;\ \xi \longrightarrow \infty.
\end{aligned}
\tag{11}
$$

The thermal results reported in Table 2 justify the numerical reflection of materials like CMS, blood, SWCNTs, and MWCNTs.

3. Prabhakar Model

Let us utilize the definition of Prabhakar model as follows:

$$
q_{(\xi,t)} = -k_\gamma\, {}^{C}\mathfrak{D}^{\gamma}_{\alpha,\beta,\alpha}\frac{\partial T_{(\xi,t)}}{\partial \xi}, \tag{12}
$$

$$
J_{(\xi,t)} = -{}^{C}\mathfrak{D}^{\gamma}_{\alpha,\beta,\alpha}\frac{\partial C_{(\xi,t)}}{\partial \xi}. \tag{13}
$$

Definition of ${}^{C}\mathfrak{D}^{\gamma}_{\alpha,\beta,\alpha}$ is as follows:

$$
\begin{aligned}
{}^{C}\mathfrak{D}^{\gamma}_{\alpha,\beta,\alpha}h(t) &= E^{-\gamma}_{\alpha,n,-\beta,\alpha}h^n(t) = e^{-\gamma}_{\alpha,n,-\beta}(\alpha;t) * h^n(t)\\
&= \int_0^t (t-\tau)^{n-\beta-1}E^{-\gamma}_{\alpha,n,-\beta}\left(\alpha(t-\tau)^{\alpha}\right)h^n(\tau)\mathrm{d}\tau\\
E^{\gamma}_{\alpha,\beta,\alpha}h(t) &= \int_0^t (t-\tau)^{\beta-1}E^{-\gamma}_{\alpha,\beta}\left(\alpha(t-\tau)^{\alpha}\right)h(\tau)\mathrm{d}\tau,
\end{aligned}
\tag{14}
$$

where

$$
E^{\gamma}_{\alpha,\beta}(z) = \sum_{m=0}^{\infty}\frac{\Gamma(\gamma+m)z^m}{m!\,\Gamma(\gamma)\Gamma(\alpha m+\beta)}. \tag{15}
$$

Using the Prabhakar's Laplace technique,

$$
\begin{aligned}
\mathscr{L}\left[{}^{C}\mathfrak{D}^{\gamma}_{\alpha,\beta,\alpha}h(t)\right] &= \mathscr{L}\left[h^m(t) * e^{-\gamma}_{\alpha,m-\beta}(\alpha;t)\right]\\
&= \mathscr{L}\{h^m(t)\}\mathscr{L}\left\{e^{-\gamma}_{\alpha,m-\beta}(\alpha;t)\right\}\\
&= \mathscr{L}\{h^m(t)\}s^{\beta-m}\left(1-\alpha s^{-\alpha}\right)^{\gamma}.
\end{aligned}
\tag{16}
$$

4. Solution Methodology via a Fractional Approach

4.1. Solution of the Heat Equation. The use of the Laplace transform on equations (9) and (12) yields

$$
\begin{aligned}
\mathrm{Pr}\ s\overline{T}_{(\xi,s)} &= -\frac{\partial \overline{q}_{(\xi,s)}}{\partial \xi},\\
\overline{q}_{(\xi,s)} &= -s^{\beta}\left(1-\alpha s^{-\alpha}\right)^{\gamma}\frac{\partial \overline{T}_{(\xi,s)}}{\partial \xi},\\
\frac{\partial \overline{T}}{\partial \xi}\bigg|_{\xi=0} &= -\left(\frac{1}{s} + \overline{T}_{(0,s)}\right);\quad \overline{T}_{(\xi,s)} \longrightarrow 0, \xi \longrightarrow \infty.
\end{aligned}
\tag{17}
$$

The solution is as follows:

$$
\overline{T}_{(\xi,s)} = \frac{1}{\sqrt{\mathrm{Pr}s^{1-\beta}/\left(1-\alpha s^{-\alpha}\right)^{\gamma}-1}}\,\frac{e^{-\xi\sqrt{\mathrm{Pr}s^{1-\beta}/(1-\alpha s^{-\alpha})^{\gamma}}}}{s}. \tag{18}
$$

The implementation framework of the Laplace transform is given in Tables 3 and 4.

4.2. Simulations for the Concentration Equation. Incorporating the Laplace algorithms to equations (10) and (13), gives

$$
\begin{aligned}
Sc\, s\overline{C}_{(\xi,s)} &= -\frac{\partial \overline{J}_{(\xi,s)}}{\partial \xi},\\
\overline{J}_{(\xi,s)} &= -s^{\beta}\left(1-\alpha s^{-\alpha}\right)^{\gamma}\frac{\partial \overline{J}_{(\xi,s)}}{\partial \xi},\\
\overline{C}_{(0,s)} &= \frac{1}{s};\quad \overline{C}_{(\xi,s)} \longrightarrow 0, \xi \longrightarrow \infty,
\end{aligned}
\tag{19}
$$

having solution:

$$
\overline{C}_{(\xi,s)} = \frac{1}{s}e^{-\xi\sqrt{Sc\, s^{1-\beta}/(1-\alpha s^{-\alpha})^{\gamma}}}. \tag{20}
$$

Table 1: Flow characteristics with mathematical expressions.

Thermal features	Mathematical representation
Effective density	$\rho_{nf} = (1-\varphi)\rho_f + \varphi\rho_s$
Dynamic viscosity	$\mu_{nf} = (\mu_f/(1-\varphi)^{2.5})$
Electrical conductivity	$\sigma_{nf} = (1+3(\sigma_s/\sigma_f - 1)\varphi/(\sigma_s/\sigma_f + 2) - (\sigma_s/\sigma_f - 1)\varphi)\sigma_f$
Thermal expansion	$(\rho\beta_T)_{nf} = (1-\varphi)(\rho\beta_T)_f + \varphi(\rho\beta_T)_s$
Heat capacitance	$(\rho C_p)_{nf} = (1-\varphi)(\rho C_p)_f + \varphi(\rho C_p)_s$
Thermal conductivity	$k_f = ((k_{CNTs} - 2\varphi(k_f - k_{CNTs}) + 2k_f)/(k_{CNTs} + 2\varphi(k_f - k_{CNTs}) + 2k_f))k_f$
Electrical conductivity	$\sigma_{nf} = \sigma_f(1+3(\sigma_s/\sigma_f - 1)\varphi/(\sigma_s/\sigma_f + 2) - (\sigma_s/\sigma_f - 1)\varphi)$

4.3. Solution for Velocity Profile. Implementing the definition of Laplace in equation (8):

$$\frac{\partial^2 \overline{u}_{(\xi,s)}}{\partial \xi^2} - \frac{1}{(1+\beta_1 s)}\left(M\sin(\theta_1) + s\right)\overline{u}_{(\xi,s)} = -\frac{Gr}{(1+\beta_1 s)}\overline{T}_{(\xi,s)} - \frac{Gm}{(1+\beta_1 s)}\overline{C}_{(\xi,s)}$$
$$\overline{u}_{(0,t)} - h\left.\frac{\partial \overline{u}}{\partial \xi}\right|_{\xi=0} = F(s); \quad \overline{u}_{(\xi,s)} \longrightarrow 0 \ \ as \ \ \xi \longrightarrow \infty. \tag{21}$$

The analytical solution is as follows:

$$\begin{aligned}\overline{u}_{(\xi,s)} = {} & \frac{1}{1+h\sqrt{(1/1+\beta_1 s)(M\sin(\theta)+s)}}\left(\frac{Gr}{1+\beta_1 s}\frac{1}{s\left(\sqrt{\left(\mathrm{Pr}s^{1-\beta}/(1-\alpha s^{-\alpha})^{\gamma}\right)}-1\right)}\frac{1+h\sqrt{\left(\mathrm{Pr}s^{1-\beta}/(1-\alpha s^{-\alpha})^{\gamma}\right)}}{\left(\mathrm{Pr}s^{1-\beta}/(1-\alpha s^{-\alpha})^{\gamma}\right)-(1/1+\beta_1 s)(M\sin(\theta)+s)}\right.\\ & \left.+\frac{Gm}{(1+\beta_1 s)s}\frac{1+h\sqrt{\left(Sc\,s^{1-\beta}/(1-\alpha s^{-\alpha})^{\gamma}\right)}}{\left(Sc\,s^{1-\beta}/(1-\alpha s^{-\alpha})^{\gamma}\right)-(1/1+\beta_1 s)(M\sin(\theta)+s)}+F(s)\right)e^{-\xi\sqrt{(1/1+\beta_1 s)(M\sin(\theta)+s)}}\\ & -\frac{Gr}{1+\beta_1 s}\frac{1}{s\left(\sqrt{\left(\mathrm{Pr}s^{1-\beta}/(1-\alpha s^{-\alpha})^{\gamma}\right)}-1\right)}\frac{1+h\sqrt{\left(\mathrm{Pr}s^{1-\beta}/(1-\alpha s^{-\alpha})^{\gamma}\right)}}{\left(\mathrm{Pr}s^{1-\beta}/(1-\alpha s^{-\alpha})^{\gamma}\right)-(1/1+\beta_1 s)(M\sin(\theta)+s)}\\ & -\frac{Gm}{(1+\beta_1 s)s}\frac{1+h\sqrt{\left(Sc\,s^{1-\beta}/(1-\alpha s^{-\alpha})^{\gamma}\right)}}{\left(Sc\,s^{1-\beta}/(1-\alpha s^{-\alpha})^{\gamma}\right)-(1/1+\beta_1 s)(M\sin(\theta)+s)}.\end{aligned} \tag{22}$$

Using the Stehfest and Tzou's algorithms, we obtain as follows:

$$w(y,t) = \frac{\ln(2)}{t}\sum_{n=1}^{N} v_n \overline{w}\left(y, n\frac{\ln(2)}{t}\right), \tag{23}$$

where

$$\begin{aligned} v_n &= (-1)^{n+(N/2)}\sum_{r=[q+1/2]}^{\min(q,(N/2))}\frac{r^{(N/2)}(2r)!}{((N/2)-r)!r!(r-1)!(q-r)!(2r-q)!},\\ w(y,t) &= \frac{e^{4.7}}{t}\left[\frac{1}{2}\overline{w}\left(r,\frac{4.7}{t}\right) + Re\left\{\sum_{j=1}^{N}(-1)^k \overline{w}\left(r,\frac{4.7+k\pi i}{t}\right)\right\}\right].\end{aligned} \tag{24}$$

Table 2: Thermal impact of CMS, blood, SWCNTs, and MWCNTs.

Material	CMC	Blood	SWCNTs	MWCNTs
$\rho\,(\mathrm{kg/m^3})$	997	1053	2600	1600
$C_p\,(\mathrm{J/kg\,K})$	4179	3594	425	796
$k\,(\mathrm{W/m\,K})$	0.613	0.492	6600	3000
$\beta_T \times 10^5\,(\mathrm{K^{-1}})$	0.9	0.18	27	44

Table 3: Numerical variation of the temperature profile at different times for different numerical algorithms.

ξ	$T(\xi,t)$ by Stehfest $t = 0.5$	$T(\xi,t)$ by Stehfest $t = 1.0$	$T(\xi,t)$ by Tzous $t = 0.5$	$T(\xi,t)$ by Tzous $t = 1.0$
0.1	1.4683	0.7295	1.4674	0.6850
0.3	1.0699	0.4734	1.0693	0.4375
0.5	0.7796	0.3031	0.7790	0.2745
0.7	0.5679	0.1909	0.5675	0.1682
0.9	0.4137	0.1176	0.4134	0.0998
1.1	0.3014	0.0703	0.3012	0.0564
1.3	0.2195	0.0402	0.2194	0.0294
1.5	0.1599	0.0213	0.1598	0.0130
1.7	0.1164	0.0099	0.1164	0.0035
1.9	0.0848	0.0031	0.0847	0.0021

Table 4: Numerical variation of the concentration field at different times for different numerical schemes.

ξ	$C_{(\xi,t)}$ by Stehfest $t = 0.5$	$C_{(\xi,t)}$ by Stehfest $t = 1.0$	$C_{(\xi,t)}$ by Tzou's $t = 0.5$	$C_{(\xi,t)}$ by Tzou's $t = 1.0$
0.1	0.8964	0.8765	0.8963	0.8757
0.3	0.7200	0.6725	0.7200	0.6707
0.5	0.5782	0.5151	0.5782	0.5125
0.7	0.4643	0.3839	0.4642	0.3909
0.9	0.3727	0.3004	0.3726	0.2975
1.1	0.2991	0.2287	0.2990	0.2258
1.3	0.2400	0.1736	0.2400	0.1710
1.5	0.1925	0.1315	0.1925	0.1290
1.7	0.1545	0.0993	0.1545	0.0971
1.9	0.1240	0.0747	0.1239	0.0728

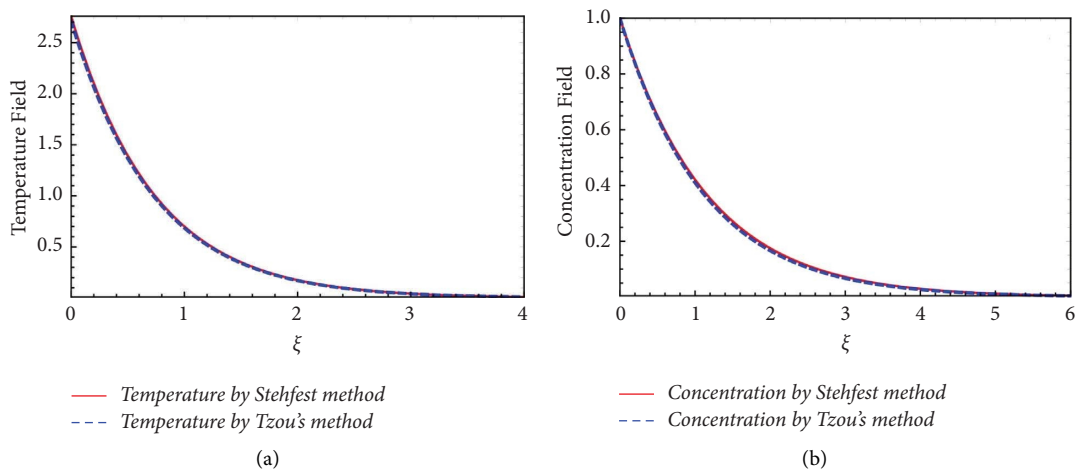

Figure 1: Graphical comparison between Stehfest and Tzou's techniques.

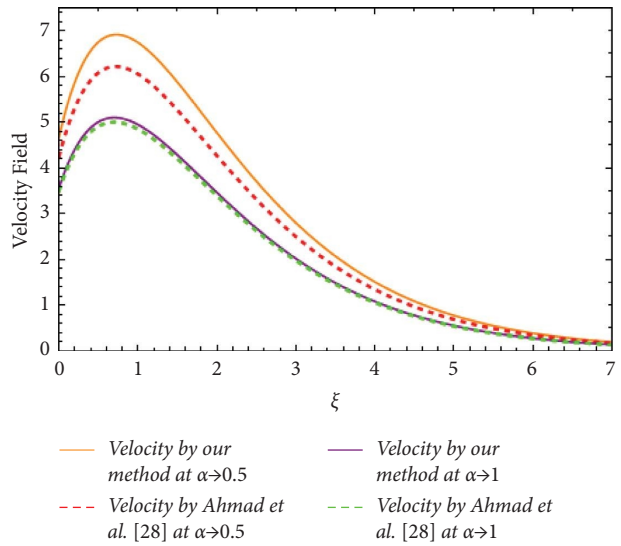

Figure 2: The comparative framework of the computed model by Ahmad et al. [28].

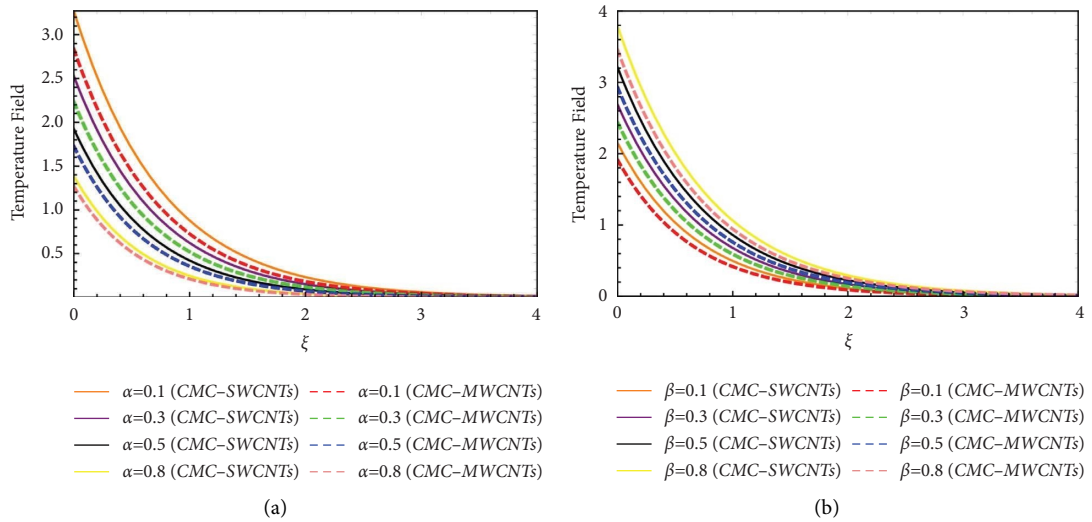

Figure 3: Temperature profile for α and β with $\gamma = 0.8, \Pr = 7.2, \varphi = 0.02$ at (a): $t = 0.8$ and (b): $t = 1.9$.

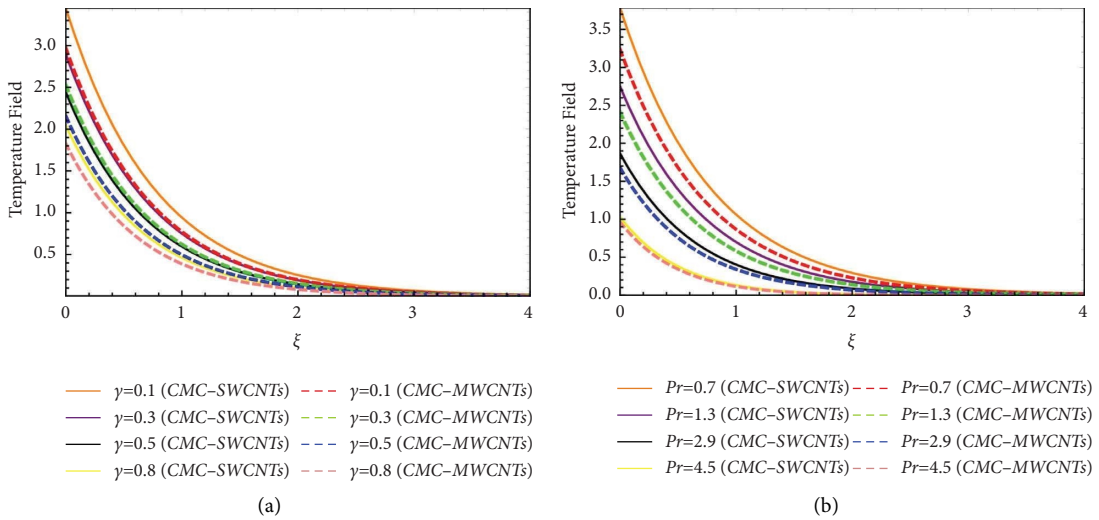

Figure 4: Variation for temperature profile with deviation in $\gamma, \Pr$ and $\alpha = \beta = 0.8, \varphi = 0.02$.

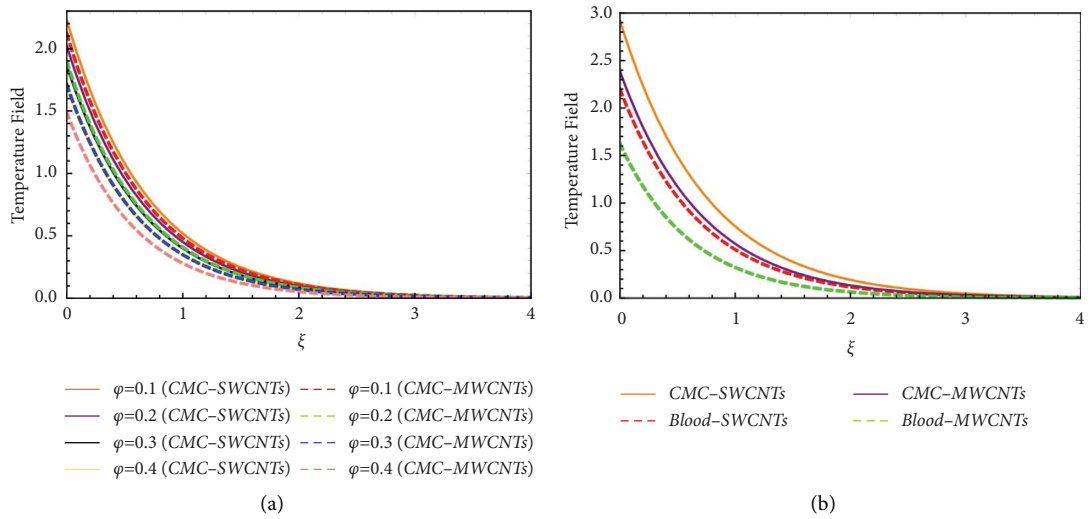

Figure 5: Variation for temperature profile with deviation in (a) volume fraction and (b) comparison of different nanoparticles.

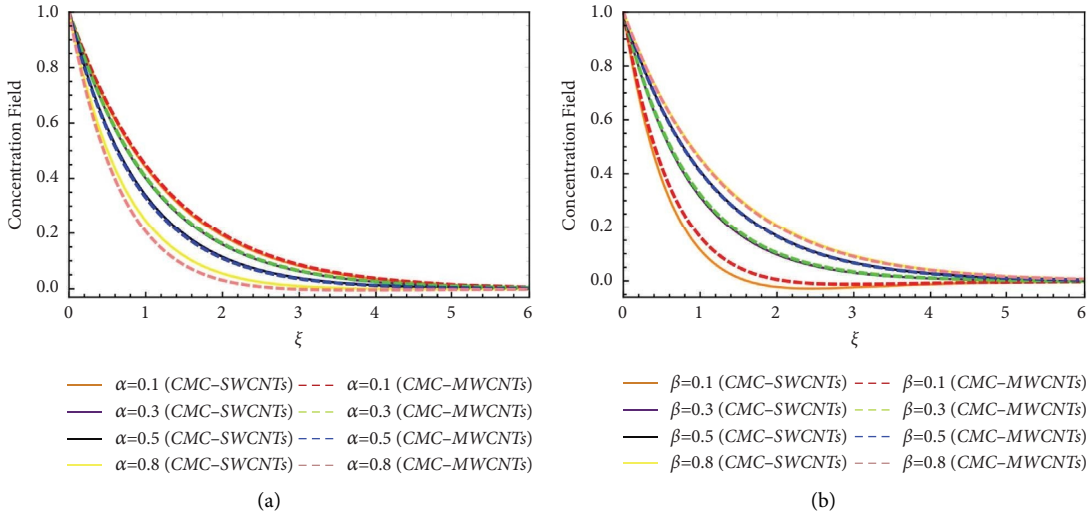

Figure 6: Variation for concentration field with deviation in α, β and $\gamma = 0.8, Sc = 5.2, \varphi = 0.02$ at (a) $t = 0.8$ and (b) $t = 1.9$.

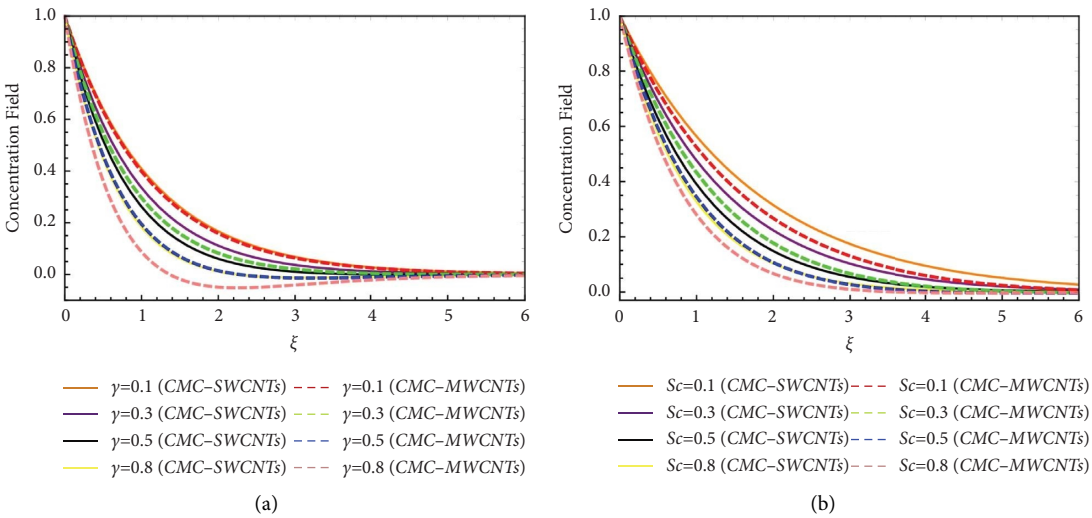

Figure 7: Variation for concentration field with deviation in γ, Sc and $\alpha = \beta = 0.8, \varphi = 0.02$.

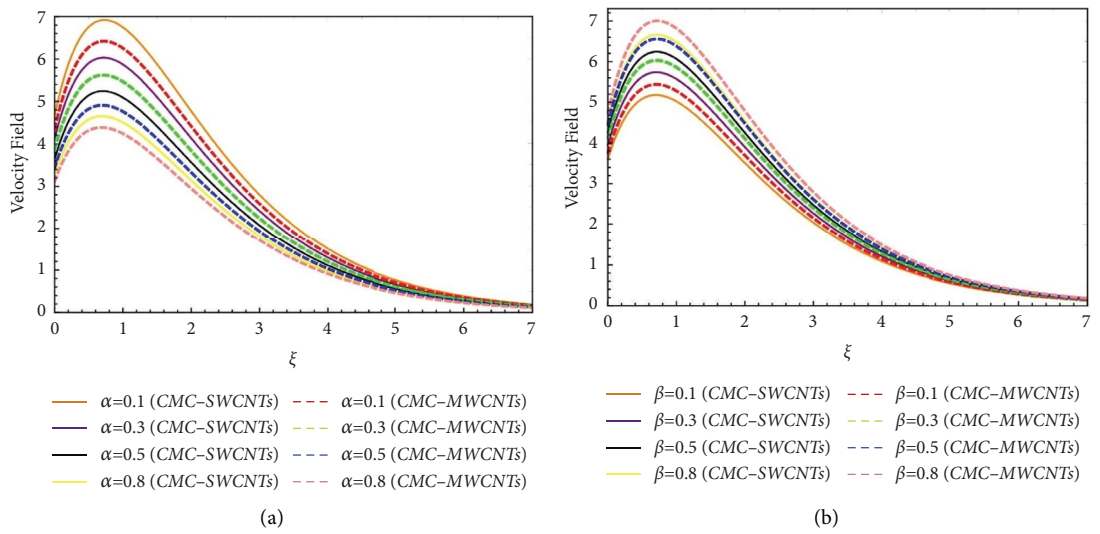

FIGURE 8: Variation for momentum profile with deviation in α, β and $\gamma = 0.8, Sc = 5.2, Gr = 4.1, Gm = 6.4, \theta = (\pi/6)$, $\Pr = 7.2, \varphi = 0.02, M = 0.6, t = 0.8$.

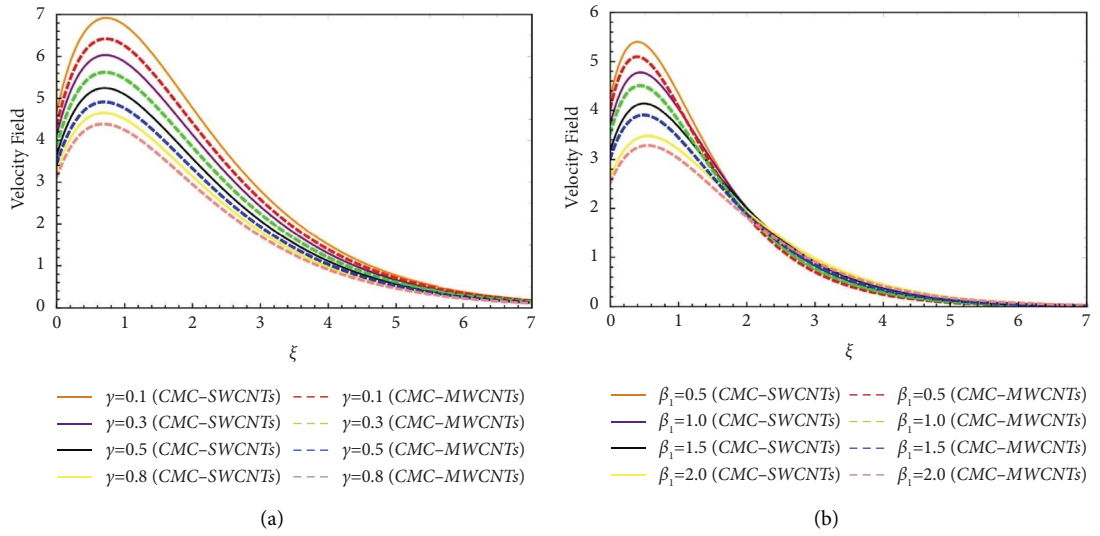

FIGURE 9: Velocity profile for γ and β_1 when $\alpha = \beta = 0.8, Sc = 5.2, Gr = 4.1, Gm = 6.4, \theta = (\pi/6), \Pr = 7.2, \varphi = 0.02, M = 0.6, t = 0.8$.

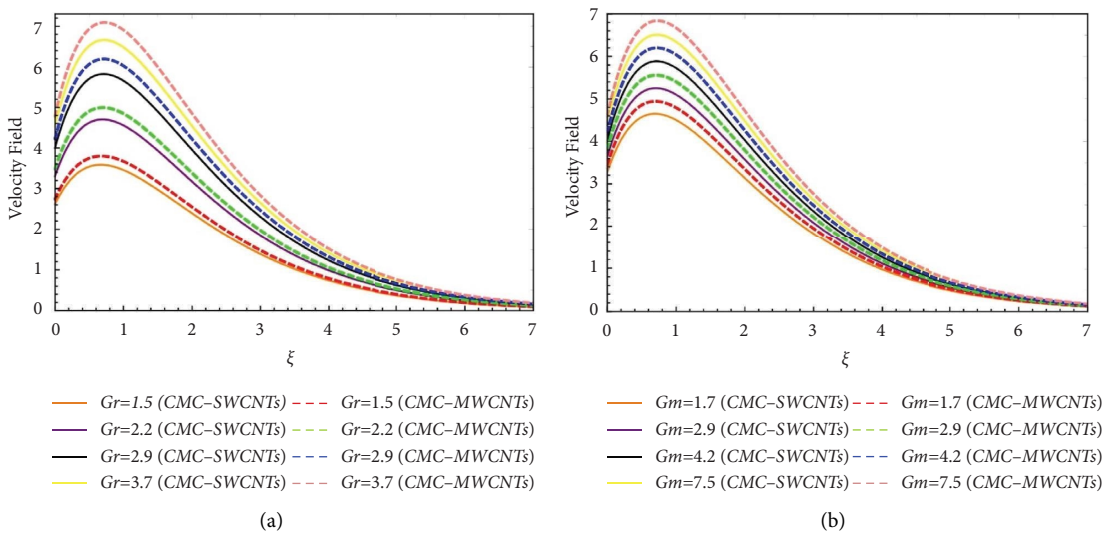

FIGURE 10: Velocity profile for Gr, Gm when $\alpha = \beta = \gamma = 0.8, Sc = 5.2, \theta = \pi/6, \Pr = 7.2, \varphi = 0.02, M = 0.6, t = 0.8$.

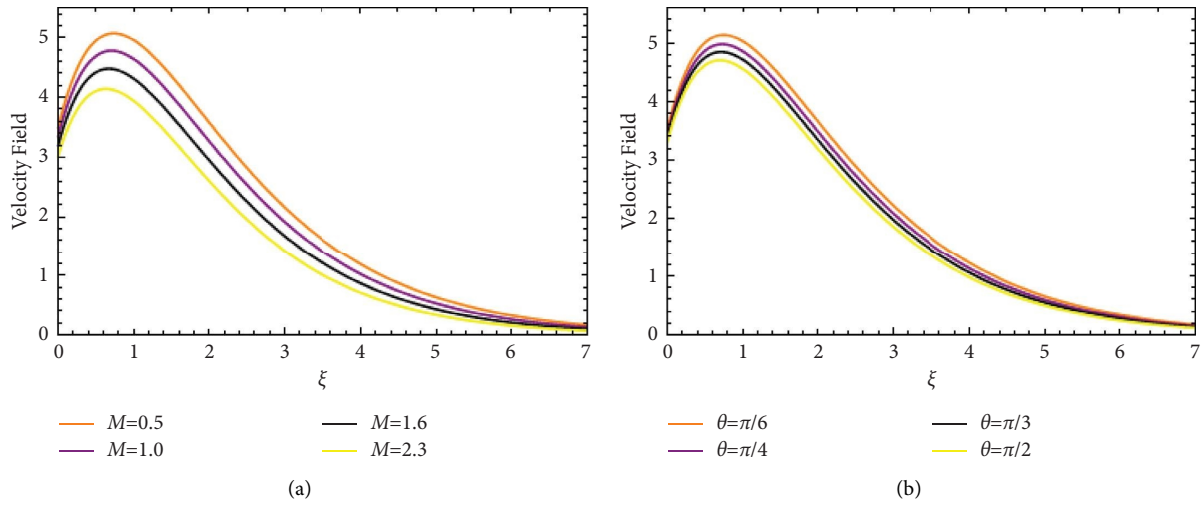

Figure 11: Velocity profile for M and θ_1 when $\alpha = \beta = \gamma = 0.8, Sc = 5.2, Gr = 4.1, Gm = 6.4, \Pr = 7.2, \varphi = 0.02, t = 0.8$.

Table 5: Numerical variation of the velocity profile at different times for different numerical schemes.

ξ	$u_{(\xi,t)}$ by Stehfest $t = 0.5$	$u_{(\xi,t)}$ by Stehfest $t = 1.0$	$u_{(\xi,t)}$ by Tzou's $t = 0.5$	$u_{(\xi,t)}$ by Tzou's $t = 1.0$
0.1	1.3577	2.8595	1.3637	2.8748
0.3	1.4143	3.2507	1.4217	3.2694
0.5	1.4125	3.4344	1.4207	3.4549
0.7	1.3706	3.4687	1.3739	3.4900
0.9	1.3025	3.3982	1.3110	3.4195
1.1	1.2184	3.2569	1.2266	3.2776
1.3	1.1256	3.0702	1.1334	3.0900
1.5	1.0296	2.8570	1.0369	2.8756
1.7	0.9341	2.6312	0.9409	2.6485
1.9	0.8418	2.4027	0.8480	2.4186

5. Validation of the Fractional Model

First, the accuracy of implemented Stehfest and Tzou's is ensured in for temperature profile and concentration profile in Figures 1(a) and 1(b), respectively. The reported results convey good agreement between both techniques. The solution based on Prabhakar's approach is validated in Figure 2 by making the comparison with work of Ahmad et al. [28]. A fine accuracy of results is noticed.

6. Discussion of Results

The physical onset due to variations in parameters is presented in this section. In order to report the more beneficiary aspect of thermal problem, the comparative results are deduced for CMC-SWCNTs, CMC-MWCNTs decomposition. Figures 3(a) and 3(b)) present the change in thermal rate due to two fractional constants α and β. The investigated analysis is inspected for CMC-SWCNTs and CMC-MWCNTs suspensions. The declining trend in temperature against α is claimed for SWCNTs and MWCNTs. However, the improvement in thermal profiles for SWCNTs and MWCNTs is noted when β varied. The thermal report due to CMC – SWCNTs is more stable when compared with CMC – SWCNTs. The observations for CMC – SWCNTs base and CMC – SWCNTs in view of fractional constant γ and Prandtl number Pr has been addressed in Figures 4(a) and 4(b). A lower temperature range for γ and Pr is noted. However, the stable heating rate for MC – SWCNTs is achieved. The controls of thermal rate due to Pr is based on the fact of low thermal diffusivity. Figure 5(a) displays the results for volume fraction φ on temperature profile in view of CMC – SWCNTs and CMC – MWCNTs nanofluid suspensions. A decreasing impact on the temperature profile with larger φ is noted. The declining change in thermal phenomenon is lower for CMC – MWCNTs. The graphical onset reported in Figure 5(b) claims a comparative thermal influence of different suspensions like –SWCNTs , blood – SWCNTs, CMC – MWCNTs and blood – MWCNTs. The thermal influence of CMC – SWCNTs has been noted as a more stable and enhancing. The lower thermal impact of blood – MWCNTs is reported. Therefore, it is concluded that the thermal impact of blood is improved by utilizing the SWCNTs. These novel observations may present many applications in health sciences, biosciences, and various engineering processes. The significance of CMC – SWCNTs and CMC – MWCNTs for concentration profile with different values of α and β has been featured in Figures 6(a) and 6(b)). Two times instants are used to compute the simulations. The enhancing and lower concentration rates are

Table 6: Numerical analysis of the local Nusselt number, Sherwood number, and skin friction.

α	Nu	Sh	C_f
0.1	1.1466	0.4338	3.2543
0.2	1.2238	0.4631	3.0731
0.3	1.3312	0.5037	2.9875
0.4	1.4735	0.5575	2.9629
0.5	1.6502	0.6244	2.9771
0.6	1.8533	0.7013	3.0154
0.7	2.0687	0.7828	3.0671
0.8	2.2805	0.8629	3.1256
0.9	2.4748	0.9364	3.1843

noted for β and α, respectively. A comparatively stable impact for CMC – SWCNT*s* is achieved. The results depicted via Figures 7(a) and 7(b) report the behavior of concentration profile for γ and *Sc*. Lower information for concentration profile is achieved for both parameters. The control of the concentration profile associated to *Sc* is due to less mass diffusivity.

Figures 8(a) and 8(b) pronounce the role of α and β on velocity profile $u(\xi, t)$. Assigning variation of α and β slows down the velocity. Figure 9(a) exhibited the change $u(\xi, t)$ for CMC – SWCNT*s* and CMC – MWCNT*s* due to γ. Here, the declining results are noted. Similar kind of lower observations are noted in Figure 9(b) where role of β_1 is justified. Figures 10(a) and 10(b) denote the contribution of *Gr* and *Gm* on profile of $u(\xi, t)$. A significant enhanced in $u(\xi, t)$ for *Gr* and *Gm* is claimed. Physically, the heat Grashof number *Gr* causes the natural convection due to buoyancy and viscous forces, and subsequently, an increment in *Gr* enhances the buoyancy forces, which results in a velocity increment. Figures 11(a) and 11(b) are prepared for assessing the contribution of magnetic parameter M and inclination angel θ for velocity profile. Both M and θ declined the velocity. The association of magnetic forces is referred to as the Lorentz force, which resists the velocity flow. Furthermore, the maximum effect of the Lorentz forces is when the angle of inclination of the applied magnetics is perpendicular to the oscillating plate.

Tables 3–6 show the results for numerical achievement based on Stehfest and Tzou's schemes. Various time instants are used to compute the simulations for accelerating phenomenon. A declining change in thermal and concentration profile for larger ξ is noted. For larger time instant, the heat and mass transfer rate is lower. From Table 6, it is observed that the Nusselt number, Sherwood number, and wall shear force declined with increasing α.

7. Conclusions

The fractional investigation is reported for the carbon nanotubes flow for suggesting the enactment in blood and carboxymethyl cellulose base liquids. For CNTs, the impacts of SWCNTs and MWCNTs are incorporated. The computational simulations are facilitated with Prabhakar's fractional scheme. The comparative thermal onset is presented. The novel findings are as follows:

(i) The suspension of CMC – SWCNT*s* and CMC – MWCNT*s* is declined for the fractional parameter.

(ii) A control of thermal decomposition of SWCNT*s* and MWCNT*s* is noted for the Prandtl number.

(iii) More stable and improved thermal impact of SWCNT*s* – CMS suspension is observed as compared to MWCNT*s* – CMS decomposition.

(iv) The concentration change enhanced was due to a fractional constant or CMC – MWCNT*s* material.

(v) The increasing trend in velocity flow is observed for mass and thermal Grashof constants.

(vi) The implemented Prabhakar fractional scheme seems to be more effective for performing the computation of different complicated problems.

Nomenclature

U: Fluid velocity (m/s)
t: Times (s)
g: Gravity acceleration (m/s^2)
K_{nf}: Thermal conductivity of the nanofluid (W/mk)
C_f: Skin friction (−)
k^*: Mean absorption parameter (−)
ρ_{nf}: Nanofluid density (kg/m^3)
U_o: Characteristic velocity (ms^{-1})
θ: Angle of magnetic inclination (−)
Pr: Prandtl number (−)
Gr: Heat Grashof number (−)
Gm: Mass Grashof number (−)
Sc: Schmidth number (−)
M: Magnetic field (−)
s: Laplace transform variable (−)
α, β, γ: Prabhakar fractional parameters (−)
B_o: Magnetic field strength (kg/s^2)
C_p: Specific heat at constant pressure (J/kgK)
μ_{nf}: Dynamic viscosity (kg/ms)
β_T: Thermal expansion coefficient (1/k)
σ: Electrical conductivity (−)
T_∞: Ambient temperature (K)
Nu: Nusselt number (−)
Sh: Sherwood number (−)
k_γ: Generalized thermal conductivity (−)
${}^{C}\mathfrak{D}^{\gamma}_{\alpha,\beta,\alpha}$: Prabhakar fractional (−).

Data Availability

All data used to support the findings of this study are available in the manuscript.

Conflicts of Interest

The authors declare that they have no conflicts of interest.

References

[1] S. Choi, "Enhancing thermal conductivity of fluids with Nanoparticles," in *Developments and Applications of Non-newtonian Flows*, D. A. Siginer and H. P. Wang, Eds., vol. 66, pp. 99–105, ASME, New York, NY, USA, 1995.

[2] M. Turkyilmazoglu, "Single phase nanofluids in fluid mechanics and their hydrodynamic linear stability analysis," *Computer Methods and Programs in Biomedicine*, vol. 187, Article ID 105171, 2020.

[3] S. Ahmad, S. Nadeem, N. Muhammad, and M. N. Khan, "Cattaneo–Christov heat flux model for stagnation point flow of micropolar nanofluid toward a nonlinear stretching surface with slip effects," *Journal of Thermal Analysis and Calorimetry*, vol. 143, no. 2, pp. 1187–1199, 2021.

[4] T. Thumma, S. R. Mishra, and O. A. Bég, "ADM solution for Cu/CuO -water viscoplastic nanofluid transient slip flow from a porous stretching sheet with entropy generation, convective wall temperature and radiative effects," *J Appl Comput Mech*, vol. 7, pp. 1291–1305, 2021.

[5] A. Abbasi, S. U. Khan, K. Al-Khaled et al., "Thermal prospective of Casson nanomaterials in radiative binary reactive flow near oblique stagnation point flow with activation energy applications," *Chemical Physics Letters*, vol. 786, Article ID 139172, January 2022.

[6] G. Rasool, A. Shafiq, and H. . Durur, "Darcy-Forchheimer relation in Magnetohydrodynamic Jeffrey nanofluid flow over stretching surface," *Discrete & Continuous Dynamical Systems - S*, vol. 14, no. 7, pp. 2497–2515, 2021.

[7] G. Rasool, A. Shafiq, S. Hussain et al., "Significance of rosseland's radiative process on reactive Maxwell nanofluid flows over an isothermally heated stretching sheet in the presence of Darcy-forchheimer and Lorentz forces: towards a new perspective on buongiorno's model," *Micromachines*, vol. 13, no. 3, p. 368, 2022.

[8] A. Shafiq, G. Rasool, H. Alotaibi et al., "Thermally enhanced Darcy-forchheimer casson-water/glycerine rotating nanofluid flow with uniform magnetic field," *Micromachines*, vol. 12, no. 6, p. 605, 2021.

[9] B. Ali, S. Hussain, M. Shafique, D. Habib, and G. Rasool, "Analyzing the interaction of hybrid base liquid C2H6O2–H2O with hybrid nano-material Ag–MoS2 for unsteady rotational flow referred to an elongated surface using modified Buongiorno's model: FEM simulation," *Mathematics and Computers in Simulation*, vol. 190, pp. 57–74, 2021.

[10] A. Mahesh, S. V. K. Varma, C. S. K. Raju, M. J. Babu, K. Vajravelu, and W. Al-Kouz, "Significance of non-Fourier heat flux and radiation on PEG – water based hybrid Nanofluid flow among revolving disks with chemical reaction and entropy generation optimization," *International Communications in Heat and Mass Transfer*, vol. 127, Article ID 105572, 2021.

[11] P. S. Reddy, P. Sreedevi, and V. N. Reddy, "Entropy generation and heat transfer analysis of magnetic nanofluid flow inside a square cavity filled with carbon nanotubes," *Chemical Thermodynamics and Thermal Analysis*, vol. 6, Article ID 100045, 2022.

[12] N. Noranuar, Q. Ahmad, S. Mohamad et al., "Non-coaxial rotation flow of MHD Casson nanofluid carbon nanotubes past a moving disk with porosity effect," *Ain Shams Engineering Journal*, vol. 12, no. 4, pp. 4099–4110, 2021.

[13] M. Imtiaz, F. Mabood, T. Hayat, and A. Alsaedi, "Impact of non-Fourier heat flux in bidirectional flow of carbon nanotubes over a stretching sheet with variable thickness," *Chinese Journal of Physics*, vol. 77, pp. 1587–1597, 2022.

[14] N. Vishnu Ganesh, Q. M. Al-Mdallal, G. Hirankumar, and R. Kalaivanan, "Impact of a hot constructal tree-shaped fin on the convection flow of single wall carbon nanotube water nanofluid inside a sinusoidal enclosure," *International Communications in Heat and Mass Transfer*, vol. 137, Article ID 106279, 2022.

[15] M. Shoaib, K. S. Nisar, M. A. Z. Raja, Y. Tariq, R. Tabassum, and A. Rafiq, "Knacks of neuro-computing to study the unsteady squeezed flow of MHD carbon nanotube with entropy generation," *International Communications in Heat and Mass Transfer*, vol. 135, Article ID 106140, 2022.

[16] F. Alzahrani and M. Ijaz Khan, "Analysis of Wu's slip and CNTs (single and multi-wall carbon nanotubes) in Darcy-Forchheimer mixed convective nanofluid flow with magnetic dipole: intelligent nano-coating simulation," *Materials Science and Engineering: B*, vol. 277, Article ID 115586, 2022.

[17] M. Caputo and M. Fabrizio, "A new definition of fractional derivative without singular kernel," *Progr Fract Differ Appl*, vol. 1, pp. 73–85, 2015.

[18] S. Momani, N. Djeddi, M. Al-Smadi, and S. Al-Omari, "Numerical investigation for Caputo-Fabrizio fractional Riccati and Bernoulli equations using iterative reproducing kernel method," *Applied Numerical Mathematics*, vol. 170, pp. 418–434, 2021.

[19] T. Zhang and Y. Li, "Exponential Euler scheme of multi-delay Caputo–Fabrizio fractional-order differential equations," *Applied Mathematics Letters*, vol. 124, Article ID 107709, 2022.

[20] A. Atangana and D. Baleanu, "New fractional derivatives with non-local and non-singular kernel: theory and application to heat transfer model," *Thermal Science*, vol. 20, no. 2, pp. 763–769, 2016.

[21] S. K. Panda, C. Ravichandran, and B. Hazarika, "Results on system of Atangana-Baleanu fractional order Willis aneurysm and nonlinear singularly perturbed boundary value problems," *Chaos, Solitons & Fractals*, vol. 142, Article ID 110390, 2021.

[22] J. Sheng, J. Wei, and D. Pang, "Finite-time stability of atangana–baleanu fractional-order linear systems," *Complexity*, vol. 2020, Article ID 1727358, 8 pages, 2020.

[23] N. Mehmood, A. Abbas, T. Abdeljawad, and A. Akgül, "Existence results for ABC-fractional differential equations with non-separated and integral type of boundary conditions," *Fractals*, vol. 29, no. 5, Article ID 2140016, 2021.

[24] J. Zhang, L. Yin, and C. Zhou, "Fractional Herglotz variational problems with Atangana–Baleanu fractional derivatives," *Journal of Inequalities and Applications*, vol. 2018, no. 1, p. 44, 2018.

[25] N. A. Shah, C. Fetecau, and D. Vieru, "Natural convection flows of Prabhakar-like fractional Maxwell fluids with generalized thermal transport," *Journal of Thermal Analysis and Calorimetry*, vol. 143, no. 3, pp. 2245–2258, 2021.

[26] A. Giusti and I. Colombaro, "Prabhakar-like fractional viscoelasticity," *Communications in Nonlinear Science and Numerical Simulation*, vol. 56, pp. 138–143, 2018.

[27] M. I. Asjad, A. Basit, A. Iqbal, and N. A. Shah, "Advances in transport phenomena with nanoparticles and generalized thermal process for vertical plate," *Physica Scripta*, vol. 96, no. 11, Article ID 114001, 2021.

[28] M. Ahmad, M. I. Asjad, K. S. Nisar, and I. Khan, "Mechanical and thermal energies transport flow of a second grade fluid with novel fractional derivative," *Part E: Journal of Process Mechanical Engineering*, Article ID 095440892110535, 2021.